J. Phys. B: At. Mol. Opt. Phys. **42** (2009) 085303 (10pp) doi:10.1088/0953-4075/42/8/085303

All-optical 3D atomic loops generated with Bessel light fields

Karen Volke-Sepúlveda and Rocío Jáuregui

Departamento de Física Teórica, Instituto de Física, Universidad Nacional Autónoma de México, A.P. 20-364, México 01000 D.F., Mexico

E-mail: karen@fisica.unam.mx and rocio@fisica.unam.mx

Received 9 February 2009, in final form 18 March 2009
Published 9 April 2009
Online at stacks.iop.org/JPhysB/42/085303

Abstract
The propagation invariance of Bessel beams as well as their transversal structure is used to perform a comparative analysis of their effect on cold atoms for four different configurations and combinations thereof. We show that, even at temperatures for which the classical description of the atom's centre-of-mass motion is valid, the interchange of momentum, energy and orbital angular momentum between light and atoms yields efficient tools for all-optical trapping, transporting and, in general, manipulating the state of motion of cold atoms.

(Some figures in this article are in colour only in the electronic version)

1. Introduction

Over the last decade, experiments on the interaction between light and cold atoms have seen tremendous advances. Laser cooling of neutral atoms is nowadays a well-established procedure, and solid steps for novel experiments in research areas such as atom optics and quantum information processing with atomic systems have been taken. During the last 15 years, the development of far-off resonance traps (FORTs) [1] has allowed the organization of cold matter in optical lattices [2] and, with this, the study of single-particle Bloch physics. The creation of trapped degenerate atomic gases, on the other hand, is one of the most exciting scientific achievements of modern times [3], as it has opened, for instance, the possibility of realizing interference of matter waves [4].

In these areas, the use of light beams with special intensity and/or phase structure yielding peculiar dynamical properties plays a very important role. Bessel beams (BB) [5], for instance, have been proposed as waveguides for atom transport due to their propagation invariance [6, 7]. The measurement of the mechanical properties of elliptical Mathieu beams could be performed through the analysis of their effects on cold atoms [8]. The transfer of orbital angular momentum (OAM) from Laguerre–Gaussian (LG) laser modes [9, 10] or high-order BBs [11–13] to cold matter has been the subject of theoretical studies in both paraxial and non-paraxial regimes. For the case of a LG beam interacting with a diatomic molecule, it was found that OAM has, in general, a weak effect on the internal state, since it becomes relevant at the electric quadrupole interaction level, while the major mechanism of exchange occurs in the electric dipole approximation and involves only the centre-of-mass motion [10]. For non-paraxial BBs interacting with a single atom, in contrast, the probability that the internal state of an atom acquires orbital angular momentum from light is maximum when the atom is located at the beam axis [13]. In fact, the helicity factor $k_z c/\omega$, which is related to the projection of angular momentum along the main direction of propagation, could be used to directly enhance or suppress atomic transitions [14].

OAM transfer is also an important aspect in the study of circular optical lattices and helical waveguides, which are interesting alternatives for interference experiments with matter waves and quantum transport. For example, Haroutyunyan and Nienhuis [15] have recently explored the use of stationary waves in the angular direction, generated by the superposition of two counter-rotating LG beams propagating in the same direction, as a more efficient alternative for achieving the exchange of angular momentum between light and cold atoms. In this case, the confinement in the radial direction could be achieved through an extra trapping potential with cylindrical symmetry, but the dynamics along the z-axis is completely free. A circular optical potential of this kind would split the wavefunction of a single localized atom into clockwise and anticlockwise components, which may interfere under certain confinement conditions [15]. Bhattacharya [16], on the other hand, presented a simplified analysis of a curved helical lattice as an atom guide, which

could be generated by the superposition of two identical LG beams propagating in opposite directions. Circular and rotating optical lattices have been studied as well, in the context of condensed matter and many particle systems, such as Fermi gases and Bose–Einstein condensates [17–21]. Moreover, ring-shaped optical lattices represent appropriated potentials for studying quasi-one-dimensional physical systems with closed-boundary conditions [18, 19]. Most of these systems consider, besides optical fields, external magnetic fields to achieve confinement in one or more spatial dimensions.

The first experimental demonstration of OAM transfer to cold atoms was reported almost a decade ago by Tabosa and Petrov [22] and, very recently, OAM was transferred to a Bose–Einstein condensate [23]. Moreover, it has been demonstrated that modes with phase singularities, as the screw-type singularity of a LG beam, in Bose–Einstein condensates are robust to decoherence effects, opening the possibility of quantum information storage in atomic vapours [24, 25].

In this work, we perform a theoretical comparative analysis of the effect of four different light fields of a circular structure on a dilute gas of cold atoms, whenever the effect of collisions among them can be neglected. In all cases, we use BBs and superpositions thereof, taking advantage of their propagation invariance property. First, we analyse the case of a single high-order BB. Second, we study the case of an optical field with $2m$ intertwined helicoidal lines of light, similar to the curved helical waveguides studied by Bhattacharya [16], but in this case, it results from superimposing two identical BBs propagating in opposite directions. In the third place, we look at a three-dimensional circular lattice, corresponding to the simultaneous generation of standing waves in the radial, angular and axial directions. As a fourth option, we analyse a circular optical lattice constituted by a collection of individual toroidal traps along the z-axis, which can be achieved by interfering two counter-propagating BBs of opposite helicity. Our interest in these particular configurations arises from the fact that they can be combined and used successively for creating 'atom loops' in predesigned ways, as will be demonstrated in the last section of this paper. Our approach follows the semiclassical description made by Gordon and Ashkin [26], which can be applied when the atom velocity is sufficiently low but not beyond the quantum limits. The quantum mechanics treatment will be presented elsewhere.

2. Rotating light beams and circular lattices

As a starting point for the present discussion, we will briefly describe the main properties of a BB within a vectorial treatment, in order to account for polarization properties. Under ideal conditions, the electromagnetic field of a Bessel mode has cylindrical symmetry, which guarantees its propagation invariance along the z-axis, in terms of its components:

$$E_\rho^\kappa = \frac{\partial^2}{\partial z \partial \rho}\Pi_\kappa^{(\mathrm{TM})} - \frac{1}{\rho}\frac{\partial^2}{c\partial t \partial \phi}\Pi_\kappa^{(\mathrm{TE})}, \tag{1}$$

$$E_\phi^\kappa = \frac{1}{\rho}\frac{\partial^2}{\partial z \partial \phi}\Pi_\kappa^{(\mathrm{TM})} + \frac{\partial^2}{c\partial t \partial \rho}\Pi_\kappa^{(\mathrm{TE})}, \tag{2}$$

$$E_z^\kappa = -\frac{\partial^2}{c^2\partial t^2}\Pi_\kappa^{(\mathrm{TM})} + \frac{\partial^2}{\partial z^2}\Pi_\kappa^{(\mathrm{TM})}, \tag{3}$$

where $\Pi_\kappa^j = \mathcal{E}_\kappa^j \psi_m(k_\perp\rho,\phi)\,\mathrm{e}^{\mathrm{i}(k_z z-\omega t)}$, with $\psi_m(k_\perp\rho,\phi) = J_m(k_\perp\rho)\,\mathrm{e}^{\mathrm{i}m\phi}$. J_m is the Bessel function of order m and $\mathcal{E}^{(\mathrm{TE})}$ ($\mathcal{E}^{(\mathrm{TM})}$) is proportional to the amplitude of the transverse electric (magnetic) mode. κ denotes collectively the parameters that define the mode, namely, the propagation wave number along the z-axis k_z, the transverse propagation wave number $k_\perp$ and the azimuthal index m.

By superpositions of TE and TM Bessel modes, different polarizations states can be obtained. In the literature [11, 27, 28], the modes,

$$\begin{aligned}\vec{E}_m^{(\mathcal{L})}(\vec{r},t;k_\perp,k_z) &= E_0^{(\mathcal{L})}\,\mathrm{e}^{\mathrm{i}(k_z z-\omega t)}\\ &\times\left[(\hat{e}_x+\mathrm{i}\hat{e}_y)\psi_m - \frac{\mathrm{i}}{2}\left(\frac{k_\perp}{k_z}\right)\psi_{m+1}\hat{e}_z\right],\\ \vec{E}_m^{(\mathcal{R})}(\vec{r},t;k_\perp,k_z) &= E_0^{(\mathcal{R})}\,\mathrm{e}^{\mathrm{i}(k_z z-\omega t)}\\ &\times\left[(\hat{e}_x-\mathrm{i}\hat{e}_y)\psi_m + \frac{\mathrm{i}}{2}\left(\frac{k_\perp}{k_z}\right)\psi_{m-1}\hat{e}_z\right],\end{aligned} \tag{4}$$

are considered to be the analogues of left-handed ($\mathcal{L}$) and right-handed ($\mathcal{R}$) circularly polarized plane wave modes. Their superpositions $\vec{E}_m^{(\mathcal{R})} \pm \vec{E}_m^{(\mathcal{L})}$ define linearly polarized modes. In terms of TE and TM modes,

$$\begin{aligned}\vec{E}_m^{(\mathcal{L})} &= E_0^{(\mathcal{L})\prime}\left(\vec{E}_{m+1}^{(\mathrm{TM})} - \mathrm{i}\frac{ck_z}{\omega}\vec{E}_{m+1}^{(\mathrm{TE})}\right)\\ \vec{E}_m^{(\mathcal{R})} &= E_0^{(\mathcal{R})\prime}\left(\vec{E}_{m-1}^{(\mathrm{TM})} + \mathrm{i}\frac{ck_z}{\omega}\vec{E}_{m-1}^{(\mathrm{TE})}\right).\end{aligned} \tag{5}$$

The mechanical properties of the photons associated with Bessel modes are directly related to the numbers ω, k_z, m that characterize them, along with the polarization. In fact, $\hbar\omega, \hbar k_z, m\hbar$ correspond to the energy, linear momentum and orbital angular momentum along the z direction respectively[1]. A linearly polarized mode has the structure

$$\begin{aligned}\vec{E}_m(\vec{r},t;k_\perp,k_z) &= E_0\,\mathrm{e}^{\mathrm{i}(k_z z-\omega t)}\\ &\times\left[(\psi_m\hat{e}_x - \frac{\mathrm{i}}{2}\left(\frac{k_\perp}{k_z}\right)(\psi_{m+1}-\psi_{m-1})\hat{e}_z\right].\end{aligned} \tag{6}$$

In what follows, we will describe in some detail each one of the four optical fields of interest, providing an explicit analytical expression and a brief discussion about their experimental generation. For this purpose, it will be useful to establish first a distinction between rotating and stationary BBs, in terms of their azimuthal dependence.

While a linearly polarized rotating BB corresponds to that given by (6), with $\psi_m(\rho,\varphi) = J_m(k_\perp\rho)\,\mathrm{e}^{\mathrm{i}m\varphi}$, a stationary BB is formed by the superposition of two rotating BBs of the same topological charge $|m|$ travelling along the same axis

[1] A superposition of TE and TM modes with equal weights $\mathbf{E}_m^{(\pm)} = E_0'(\mathbf{E}_{m+1}^{(\mathrm{TM})} \pm \mathrm{i}\mathbf{E}_{m+1}^{(\mathrm{TE})})$, corresponds to photons with a helicity, i.e., a projection of the spin angular momentum along the z-axis of $\pm\hbar k_z c/\omega$. In the paraxial limit, this superposition coincides with the definition of circular polarized beams through equations (5).

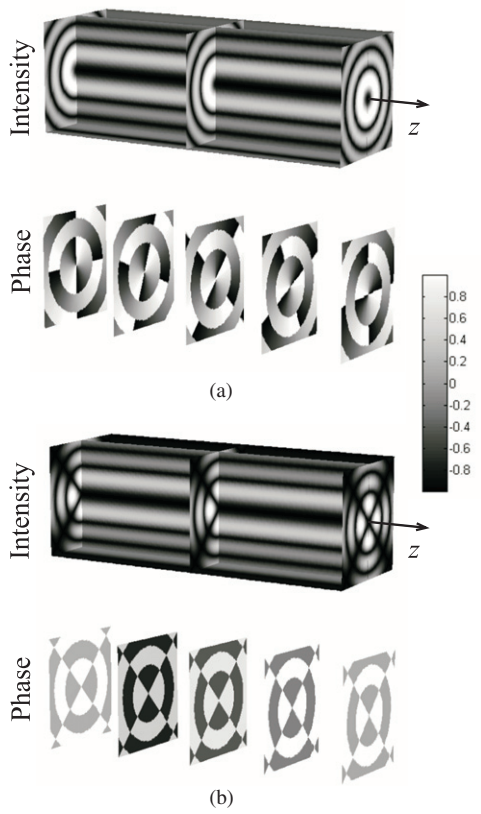

Figure 1. Comparison between (a) a rotating and (b) a stationary Bessel beam of order $m = 2$. The phase values for both beams are indicated in the colour bar on the right-hand side, in units of π radians. Along the propagation axis, both beams have a similar behaviour due to their ideal propagation invariance.

and direction, but rotating in opposite sense ($\pm m$), giving rise to

$$\vec{E}_m(\vec{r},t) = E_0\,\mathrm{e}^{\mathrm{i}(k_z z-\omega t-\varphi_0)}\Big[J_m(k_\perp\rho)\cos(m\varphi+\varphi_0)\hat{e}_x - \frac{\mathrm{i}}{2}\frac{k_\perp}{k_z}(J_{m+1}(k_\perp\rho)\cos[(m+1)\varphi+\varphi_0] - J_{m-1}(k_\perp\rho)\cos[(m-1)\varphi+\varphi_0])\hat{e}_z\Big]. \quad (7)$$

Here and in the following, $\varphi_0 = 0$ ($\varphi_0 = \pi/2$) stands for even (odd) values of m. Figure 1(a) illustrates the intensity and phase distributions of an ideal rotating BB, while figure 1(b) shows the same for an ideal stationary BB; in both cases $m = 2$. It is seen that the ideal fields exhibit propagation invariance of their intensity along the z-axis.

Note that the term 'rotating beam' can be found in the literature with a different meaning. In [29, 30], this term refers to paraxial beams that are forcibly rotated around the propagation axis by superposing components with a well-defined angular momentum $\hbar m$ per photon, each having a frequency shift m times the rotation frequency. These light distributions are time dependent and possess interesting properties on their own. Their interactions with atoms deserve an independent study.

The optical fields of interest will be constructed as superpositions of linearly polarized Bessel modes in the sense discussed above, either rotating or stationary, with the transverse component of their electric fields oriented along the x-axis.

Case 1: single rotating Bessel beam

A single BB in interaction with cold atoms has been studied before [6, 7, 13]. Here we include this simple case for comparative purposes with the other configurations and also to emphasize some of its applications for controlling atomic motion. The expression for a linearly polarized rotating BB is, according to (6),

$$\vec{E}^{(1)}_m(\vec{r},t;k_\perp,k_z) = E_0\,\mathrm{e}^{\mathrm{i}(k_z z+m\varphi-\omega t)}\Big[J_m(k_\perp\rho)\hat{e}_x - \frac{\mathrm{i}}{2}\frac{k_\perp}{k_z}(J_{m+1}(k_\perp\rho)\,\mathrm{e}^{\mathrm{i}\varphi} - J_{m-1}(k_\perp\rho)\,\mathrm{e}^{-\mathrm{i}\varphi})\hat{e}_z\Big]. \quad (8)$$

Experimentally, reasonable approximations to BBs of different orders have been efficiently generated by illuminating an axicon or conical lens with a single-ringed Laguerre–Gaussian mode of order m [31]. Another approach is to obtain the desired BB directly from properly designed computer-generated holograms (CGH) [32], which can be displayed in spatial light modulators (SLM) [33]. The original setup proposed by Durnin and coworkers [5], consisting of a dark screen with a thin annulus transmittance function placed at the back focal plane of a positive lens, turns out to be inefficient for optical trapping experiments, although it is the best approximation to the theoretical expression. In all cases, of course, BBs can be generated only within a *finite* region and, under current experimental conditions, the paraxial approximation is generally fulfilled. It is worth mentioning, however, that BBs with relatively large transverse dimensions ($k_\perp/k_z \ll 1$) can be reduced with additional lenses in order to make them more suitable for atom trapping experiments.

Case 2: twisted helical lattice

This field can be generated by the interference of two rotating BBs with the same helicity but propagating in opposite directions. This means that the two beams have the same projection of their respective angular momenta along their own propagation direction but, with respect to the same and fixed reference frame, they are rotating in opposite directions, as illustrated in figure 2. The resulting field is described by

$$\vec{E}^{(2)}_m(\vec{r},t) = E_0\,\mathrm{e}^{-\mathrm{i}(\omega t+\varphi_0)}\Big[J_m(k_\perp\rho)\cos(m\varphi+k_z z+\varphi_0)\hat{e}_x - \frac{\mathrm{i}}{2}\left(\frac{k_\perp}{k_z}\right)(J_{m+1}(k_\perp\rho)\cos[(m+1)\varphi+k_z z+\varphi_0] - J_{m-1}(k_\perp\rho)\cos[(m-1)\varphi+k_z z+\varphi_0])\hat{e}_z\Big]. \quad (9)$$

The experimental generation of this optical field can be performed by introducing a rotating BB into an amplitude division interferometer; each portion of the split beam should suffer the same number of reflections, so that the helicity is preserved for both of them before being superimposed again along the same axis while propagating in opposite directions.

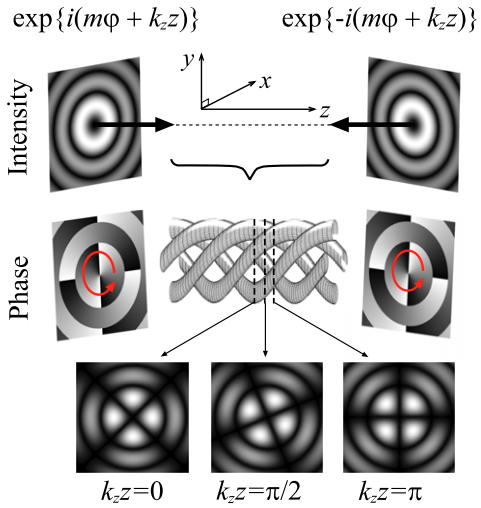

Figure 2. Schematic of the superposition of two rotating BBs propagating in opposite directions; the rotation sense of the beams is opposite as well with respect to the same fixed reference frame. Transverse cross sections of the resulting field at different z planes indicate an intensity distribution that is twisted around the z-axis, but stationary in time. The whole structure resembles a rope with $2m$ main inner strands of light twisted together and outer groups of strands with reduced intensity.

Case 3: 3D stationary circular lattice

In this case, we consider the interference of two stationary Bessel modes of the type described by (7), but propagating in opposite directions along the same z-axis. The resulting optical field will exhibit standing waves in all the three spatial dimensions within a circular cylindrical geometry:

$$\vec{E}_m^{(3)}(\vec{r},t) = E_0\,\mathrm{e}^{-\mathrm{i}(\omega t+\varphi_0)}\cos(k_z z)\Big[J_m(k_\perp\rho)\cos(m\varphi+\varphi_0)\hat{e}_x - \frac{\mathrm{i}}{2}\frac{k_\perp}{k_z}(J_{m+1}(k_\perp\rho)\cos[(m+1)\varphi+\varphi_0] - J_{m-1}(k_\perp\rho)\cos[(m-1)\varphi+\varphi_0])\hat{e}_z\Big]. \quad (10)$$

Intensity nodal surfaces correspond, along the radial direction, to concentric dark cylinders whose radii $\rho = \rho_{mn}$ are defined by $k_\perp\rho_{mn} = x_{nm}$, with x_{mn} the nth root of the Bessel function of order m. The cylinders are intersected by $2|m|$ semi-infinite nodal planes along the azimuthal coordinate, defined by $[|m|\,\varphi_n + \varphi_0] = (2n-1)\pi/2$, where $n = 1, 2, \ldots, 2|m|$. Finally, there are also nodal planes along the z-axis corresponding to $z_n = (2n-1)\lambda_z/4$, with n being an integer and $\lambda_z = 2\pi/k_z$. The experimental generation of a lattice like this may involve two steps. First, it is necessary to obtain the stationary BB, which can be done either directly, by means of a CGH, or by interfering two counter rotating BBs propagating along the same axis and direction, for instance. Once obtained the stationary BB, an amplitude division interferometer would be appropriated for superimposing two equally weighted portions of it, aligned along the same axis, but propagating in opposite directions. This is schematically illustrated in figure 3.

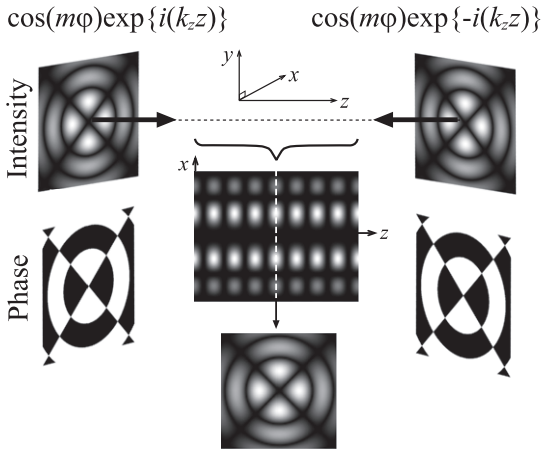

Figure 3. Schematic of the superposition of two stationary BBs propagating in opposite directions. Standing waves are generated in the three spatial directions: radial, angular and axial.

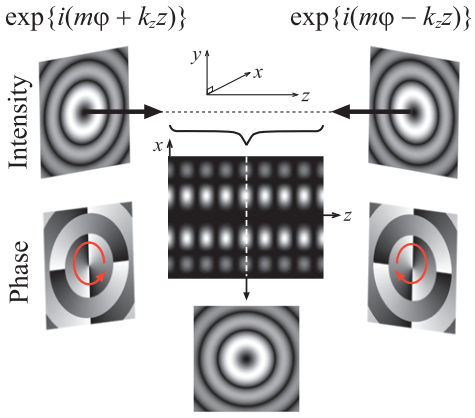

Figure 4. Schematic of the superposition of two rotating BBs propagating in opposite directions; the rotation sense of the beams in this case is the same with respect to the same fixed reference frame. The 3D intensity distribution would resemble a straight backbone of light.

Case 4: toroidal train lattice

A set of toroidal traps along an axis can be generated by the interference of two rotating BBs with opposite helicities and propagating in opposite directions. This means that the two beams have opposite projections of their respective angular momenta along their own propagation direction but, with respect to the same reference frame, they are rotating in the same direction, as illustrated in figure 4. The resulting field is given by

$$\vec{E}_m^{(4)}(\vec{r},t) = E_0\,\mathrm{e}^{\mathrm{i}(m\varphi-\omega t)}\cos(k_z z)\Big[J_m(k_\perp\rho)\hat{e}_x - \frac{\mathrm{i}}{2}\Big(\frac{k_\perp}{k_z}\Big) \times [J_{m+1}(k_\perp\rho)\,\mathrm{e}^{\mathrm{i}\varphi} - J_{m-1}(k_\perp\rho)\,\mathrm{e}^{-\mathrm{i}\varphi}]\hat{e}_z\Big]. \quad (11)$$

A transverse cross section of this field at an antinodal plane along the z-axis is exactly the same that the transverse cross section of a propagating rotating BB, but null intensity occurs at the z nodal planes which, as in case 3, correspond to the planes $z_n = (2n-1)\lambda_z/4$ (n integer). The experimental

Table 1. Coupling factor $\tilde{g}$, and conservative $\vec{\alpha}$ and dissipative $\vec{\beta}$ vectors defining the atom–BB interaction, expression (14) for the different beam configurations described in section 2.

Case	$\tilde{g}$	$\vec{\alpha}$	$\vec{\beta}$
1	$J_m(k_\perp\rho)\,\mathrm{e}^{\mathrm{i}(k_z z+m\varphi)}$	$k_\perp \frac{J'_m(k_\perp\rho)}{J_m(k_\perp\rho)}\hat{e}_\rho$	$\frac{m}{\rho}\hat{e}_\varphi + k_z\hat{e}_z$
2	$J_m(k_\perp\rho)\cos(k_z z+m\varphi)$	$k_\perp \frac{J'_m(k_\perp\rho)}{J_m(k_\perp\rho)}\hat{e}_\rho - (\frac{m}{\rho}\hat{e}_\varphi + k_z\hat{e}_z)\tan(m\varphi+k_z z)$	$\vec{0}$
3	$J_m(k_\perp\rho)\cos(k_z z)\cos(m\varphi)$	$k_\perp \frac{J'_m(k_\perp\rho)}{J_m(k_\perp\rho)}\hat{e}_\rho - \frac{m}{\rho}\tan(m\varphi)\hat{e}_\varphi - \tan(k_z z)\hat{e}_z$	$\vec{0}$
4	$J_m(k_\perp\rho)\cos(k_z z)\,\mathrm{e}^{\mathrm{i}m\varphi}$	$k_\perp \frac{J'_m(k_\perp\rho)}{J_m(k_\perp\rho)}\hat{e}_\rho - k_z\tan(k_z z)\hat{e}_z$	$\frac{m}{\rho}\hat{e}_\varphi$

generation of this optical field can be performed by introducing a rotating BB into an amplitude division interferometer; one portion of the split beam should suffer an extra reflection, so that its helicity is inverted with respect to the other portion of the beam before joining them together along the same axis while propagating in opposite directions.

As we shall see in the following section, Bessel optical modes, either stationary or propagating, exhibit interesting features in the interaction with cold atoms, due to their propagation invariance property and their multiringed radial structure.

3. The semiclassical description of a single atom motion within the light field

We take the standard semiclassical description as in the pioneer works by Letokhov and coworkers [34], and Gordon and Ashkin [26]. In this approximation, a monochromatic electromagnetic wave describable by a coherent state couples to the dipole moment of an atom. This dipole moment $\vec{\mu}_{12}$ is related to the electromagnetic transitions between the atom levels that, for simplicity, will be taken to have just two accessible options. The coupling, $g = \mathrm{i}\vec{\mu}_{12}\cdot\vec{E}/\hbar$, depends explicitly on the orientation of the electric field $\vec{E}$ of the wave. For the systems described in this work, $\vec{E}$ arises from linearly polarized beams and has a longitudinal component that is much smaller than the transverse component (paraxial light fields) since $k_z \gg k_\perp$. As a consequence, from now on, the effect of longitudinal fields on the atom will be neglected, and we can take the coupling factor as

$$g \sim \mathrm{i}\vec{\mu}_{12}\cdot\vec{E}_\perp/\hbar = [\mathrm{i}(\vec{\mu}_{12}\cdot\hat{e}_x)E_0/\hbar]\tilde{g}(\rho,\varphi,z), \qquad (12)$$

where $\tilde{g}$ contains the information about the spatial structure of the light field. The force exerted by a light field on a slowly moving neutral atom is, in the first approximation, proportional to the gradient of the coupling factor,

$$\nabla g = (\vec{\alpha} + \mathrm{i}\vec{\beta})g. \qquad (13)$$

Here we have used that $g = |g|\exp(\mathrm{i}\phi)$, and hence $\vec{\alpha} = \vec{\nabla}\ln|g|$ and $\vec{\beta} = \vec{\nabla}\phi$. These vectors are related to conservative and dissipative terms in the interaction force, respectively, as we shall see in the following. In table 1, the spatial structure factor $\tilde{g}(\rho,\varphi,z)$ associated with the different beam configurations is given along with the force factors $\vec{\alpha}$ and $\vec{\beta}$.

If the kinetic energy of the atom is low enough to be sensitive to the optical force but large enough to admit a classical description in terms of Newton equations, the expression for the average semiclassical velocity-dependent force [26], valid for both propagating and standing beams, is

$$\langle\vec{f}\rangle = \hbar\tilde{\Gamma}p'[[(\vec{v}\cdot\vec{\alpha})(1-p)(1+p)^{-1} + \Gamma/2]\vec{\beta} + [(\vec{v}\cdot\vec{\beta}) - \delta\omega]\vec{\alpha}]. \qquad (14)$$

In this expression

$$\tilde{\Gamma} = \Gamma/[\Gamma(1+p') + 2\vec{v}\cdot\vec{\alpha}[1 - p/p' - p][p'/(1+p)]], \qquad (15)$$

where $\Gamma = 4k^3|\vec{\mu}_{12}|^2/3\hbar$ is the Einstein coefficient, $\delta\omega = \omega - \omega_0$ denotes the detuning between the wave frequency ω and the transition frequency ω_0, $p = 2|g|^2((\Gamma/2)^2 + \delta\omega^2)$ is known as the saturation parameter, linked to the difference D between the populations of the two levels of the atom, $D = 1/(1+p)$, and finally $p' = 2|g|^2/|\gamma'|^2$, with $\gamma' = (\vec{v}\cdot\vec{\alpha})(1-p)(1+p)^{-1} + \Gamma/2 + \mathrm{i}((\vec{v}\cdot\vec{\beta}) - \delta\omega)$.

Although the dissipative term $(\vec{v}\cdot\vec{\beta})$, associated with a Doppler shift, as well as other velocity-dependent terms in (14) is expected to be very small for slow atoms, we will keep them in our numerical calculations in order to prevent disregarding of potentially relevant effects, since the atom may increase its kinetic energy as in interacts with the light beam.

In experiments with cold atoms, it is well known that gravity effects should, in general, be taken into account to describe accurately their motion. Here, we will consider that the z-axis of the light field configurations is oriented along the vertical direction. The atoms are downloaded to the optical trap, with most of their kinetic energy coming from the axial velocity which is assumed, unless otherwise stated, to be negative.

4. Numerical results

In this work, as we are interested in optical lattices, we will consider red-detuned far-off resonance light beams. The bright regions of the light intensity distribution correspond to minima of the effective potential energy V_{eff} associated with the term $\vec{\alpha} = -\vec{\nabla}V_{\mathrm{eff}} = \vec{\nabla}\ln|g|$. The behaviour of the atom in the light field depends not only on its initial balance between kinetic and effective potential energy, but also on its initial momentum and position. In all the studied cases, we will illustrate the behaviour of an atomic cloud, which means that we will show the paths of several atoms whose initial conditions vary within a certain range of experimentally accessible values.

The parameters in the numerical simulations consider ^{85}Rb atoms. Following [1], the laser beam is considered with a

detuning of 67 nm to the red of the $5\,^2S_{1/2}$–$5\,^2P_{1/2}$ transition at 795 nm and an irradiance of 6 mW μm^{-2} that determines the value of the coupling constant $|\vec{\mu}_{12} \cdot E_0 \hat{e}_x|/\hbar$. The trajectories of the atoms are described by taking the laser wavelength as unit of length and, as unit of time, the inverse of the Einstein coefficient Γ which, for the $5\,^2P_{1/2}$ state of ^{85}Rb, is 3.7×10^7 s^{-1}. The initial kinetic energies are reported in terms of the corresponding 'temperature' by dividing by the Boltzmann constant k_B. Although we have analysed several values of the light field characteristic parameters, in order to be specific we report just the results where $k_z = 0.995\omega/c$ and the topological charge $m = 2$. This makes a paraxial realization of the beam a good approximation, and admits the possibility of observing light–atom angular momentum transfer.

In the reported clouds, the range of initial conditions of the atoms is: $0.01\lambda \leqslant \rho \leqslant 2.6\lambda, 0.0001\lambda \leqslant z \leqslant 0.001\lambda, -0.0001\lambda\Gamma \leqslant \dot{\rho} \leqslant 0.0001\lambda\Gamma, 0.0001\Gamma \leqslant \dot{\varphi} \leqslant 0.00015\Gamma, -0.0025\lambda\Gamma \leqslant \dot{z} \leqslant -0.001\lambda\Gamma$ with the initial kinetic energies ranging from $\sim$5 μK to $\sim$30 μK.

Case 1: single rotating Bessel beam

The optical potential energy linked to the conservative factor $\vec{\alpha}$, in this case consists of annular potential wells, corresponding to the concentric bright rings of the intensity distribution of the BB. An atom trapped in one of the bright rings of the beam oscillates in the radial direction around the minimum of the potential energy with an amplitude that depends on its initial position and velocity. Along the z-axis, the atom is subjected to the gravity force and to the dissipative term $\vec{\beta}$ of the optical force, associated with the phase of the light field $\vec{\beta} = \vec{\nabla}\phi$. In a FORT with the parameters given above, the dissipative effects have small influence on the atom's motion. Hence, the gravity force dominates the evolution along the z-axis and the transfer of orbital angular momentum from the beam to the atom is also negligible. The smaller the detuning, the larger the effect of the dissipative forces, so that the optical acceleration along the azimuthal and axial directions would eventually become noticeable.

Figure 5 illustrates some of the typical trajectories for atoms of the cloud described above and downloaded in a second-order BB at $z \simeq 0$. Although the light beam is propagating upwards, the atoms move downwards due to their initial negative velocities and to the acceleration of gravity. Gravity also helps to keep the atoms stably trapped within the beam profile in the transverse direction, even if the initial radial position of an atom is close to the axial node ($\rho \sim 0.01\lambda$). In contrast, we have verified that some atoms would escape in the radial direction if the atomic cloud were considered with similar initial conditions but with positive sign of the z-component of the velocity. In figure 5(b), we also show the angular momentum as a function of time for each of the atoms illustrated in figure 5(a). In all the cases, the angular momentum remains practically equal to its initial value.

Single rotating BBs have been proposed before as guides for cold atoms [6, 7] though no semiclassical calculations were reported. Here, we have considered a red-detuned system and found that a BB may, indeed, be used as an atom guide in this case.

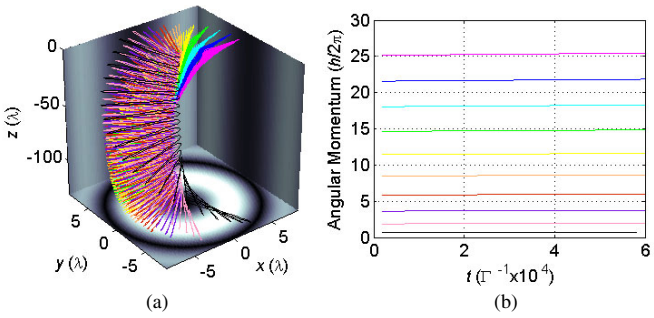

Figure 5. (a) Illustrative spatial paths of some of the atoms in the cloud described in the text moving within a rotating BB. The topological charge of the BB is $m = 2$ (positive helicity), and it is propagating along the positive z-axis (upwards direction); the axial and transverse components of its wave vector are $k_z = 0.995k$ and $k_\perp = 0.0999k$. The wavelength of the light is $\lambda = 862$ nm, which is the length unit in the plots. The smallest value of the kinetic energy and the largest absolute value of the potential energy correspond to the magenta path, whereas the opposite occurs for the black path. The starting point of all the paths is the plane $z \simeq 0$. Note the scale differences between the three spatial axes. (b) Angular momentum as a function of time for the same atoms. The range of initial conditions of the atoms in the analysed cloud is: $0.01\lambda \leqslant \rho \leqslant 2.6\lambda, 0.0001\lambda \leqslant z \leqslant 0.001\lambda, -0.0001\lambda\Gamma \leqslant \dot{\rho} \leqslant 0.0001\lambda\Gamma, 0.0001\Gamma \leqslant \dot{\varphi} \leqslant 0.00015\Gamma, -0.0025\lambda\Gamma \leqslant \dot{z} \leqslant -0.001\lambda\Gamma$) with the initial kinetic energies ranging from $\sim$5 μK to $\sim$30 μK. The colours of the illustrative paths in (a) are directly correlated to the angular momentum in (b). Animations of the different atom trajectories for all the cases treated in this study can be found in [35].

Case 2: twisted helical lattice

The intensity distribution for this case is illustrated in figure 2. A transverse cross section looks like a stationary BB, but it is rotating as a whole along the z-axis, completing a revolution in a distance of $|m|\,\lambda_z$. For a red-detuned lattice, the potential energy minima correspond to a set of $2\,|m|$ twisted intertwined pipes between each pair of radial nodes, along which the atoms can be guided in independent channels. This light configuration is analogous to that proposed by Bhattacharya [16] for LG beams. However, for BB beams, the propagation invariance introduces additional features for atom guiding with respect to LG beams.

Since the axial and azimuthal variables appear in the combination $(m\varphi + k_z z)$, the light field amplitude has a well-defined helicity. In the absence of gravity, it is expected that an atom initially moving with the same helicity than that of the light pattern will preserve it, although its angular momentum may change in magnitude. Otherwise, if an atom has an initial motion with different helicity than that of the light pattern, the optical force might be able to change the atom's helicity. This fact has been verified numerically and it is illustrated in figure 6, which corresponds to (a) loading an atom cloud at the $z \simeq 0$ plane with the parameters mentioned above, so that the atoms initially move downwards and the atoms and the light pattern have the same helicity; (c) loading an atom cloud also downwards with the same parameters mentioned above with the exception of $\dot{\varphi}$ whose sign has been reversed, $-0.0015\Gamma \leqslant \dot{\varphi} \leqslant -0.001\Gamma$, so that atoms and light pattern have initially opposite helicity. In the latter case, the light

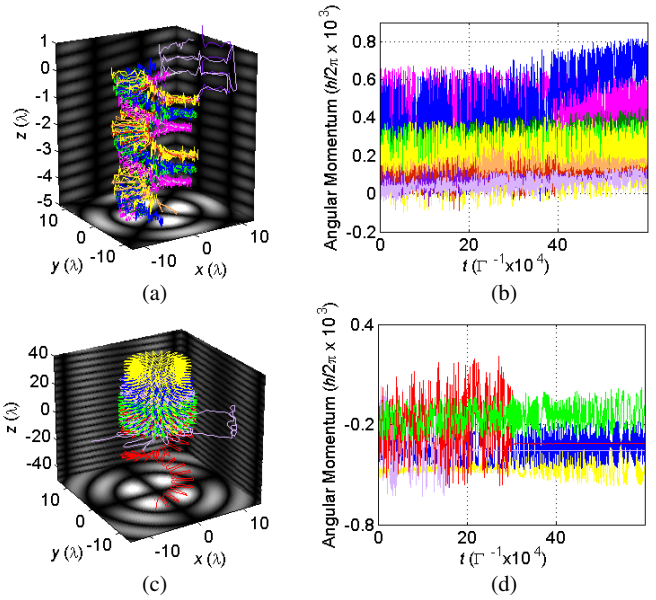

Figure 6. (a) Illustrative examples of the spatial trajectory and (b) angular momentum of atoms moving within a twisted helical Bessel lattice generated in the way described in figure 2. The parameters of the two superimposing beams and the range of initial conditions of the atoms in the analysed cloud are the same as those of figure 5 so that the atom's motion is initially downwards and has the same helicity as the light pattern. In figure (a) the time interval corresponds to $0 < T < 0.5 \times 10^4\ \Gamma^{-1}$. Figure (c) shows illustrative examples of the spatial trajectory and (d) angular momentum of atoms moving within the same twisted Bessel lattice than in (a); the initial conditions of the atoms in the analysed cloud are the same as those used in (a) but with the angular velocity $\dot{\varphi}$ reversed. Notice the scale difference in the axial coordinate in figures (a) and (c). The colours of the illustrative paths in (a) and (c) are directly correlated to the angular momentum in (b) and (d).

force attempts to change the helicity of the atoms by sending them upwards acting against gravity; when it is not able to do so, the atom exhibits a complicated trajectory that may end with its escape. Note that in both cases (a) and (c), some atoms are able to escape from the radial confinement in the Bessel ring, in particular when they are initially located close to or at a nodal surface; however, they may be eventually trapped at higher radii. The time-dependent angular momentum of each atom in both clouds has strong oscillations with an increasing average value, as illustrated in figures 6(b) and (d). For atoms with an helicity coinciding with that of the light pattern, an average angular momentum that starts being $10\hbar$, as in case 1, ends with values up to $5 \times 10^2\hbar$ for $t \sim 10^5\ \Gamma^{-1}$.

These results show that: (i) twisted helical beams act as waveguides with intertwined channels that determine the rotation direction of radially trapped atoms, and (ii) a significant amount of angular momentum can be transferred to atoms using this beam configuration.

Case 3: 3D stationary circular lattice

The intensity distribution of this lattice (figure 3) corresponds to a set of individual 'potential cages' (potential wells in all the three spatial dimensions) distributed around in a coordinate system with circular cylindrical geometry. Nodal surfaces define the limits of the potential cages. The

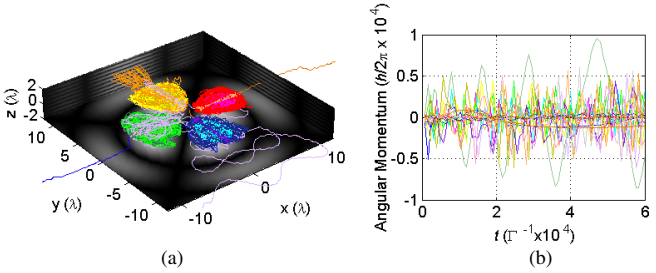

Figure 7. (a) Spatial paths of atoms moving within a 3D Bessel lattice generated by the superposition of two stationary BBs of second order propagating in opposite directions, as described in figure 3. (b) Angular momentum as a function of time for the same atoms. The parameters of the two superimposing beams and the range of initial conditions of the atoms in the analysed cloud are the same as those of figure 5. The colours of the illustrative paths in (a) are directly correlated to the angular momentum in (b).

numerical simulation with the cloud described above shows that: (i) atoms initially located at a nodal surface have a high probability of escaping from the lattice due to the lack of potential energy, particularly when they are very close to the axis of symmetry of the beam; (ii) for atoms initially located within a cage, so that their total initial energy is negative, the trapping in this lattice results very robust, regardless of the direction of its initial momentum and in spite of the presence of gravity. In some is, depending on its initial position and velocity, an atom may tunnel from one cage to the next one either along the axial or the azimuthal direction, while keeps confined in the other directions. In the latter case, the atom may stay trapped in a transverse plane, going around the whole beam circumference. Illustrative examples of trajectories for the atomic cloud described above are given in figure 7.

In figure 7, we also observe fluctuations of the orbital angular momentum L_z at least one order of magnitude larger than the results for the twisted helical configuration; figure 6. These fluctuations are associated with the confinement in all directions. Note that in this case, the mean axis of rotation of each atomic trajectory is located in the cages, so that it does not coincide with the axis of the beam.

Based on the high angular momentum oscillations, we consider that this kind of lattice might be especially interesting in the study of vortices in degenerate gases. Note as well that it would be a more appropriate choice for the studies of quasi-one-dimensional systems with periodic boundary conditions along the azimuthal direction proposed by Amico and coworkers [18], since the scheme they proposed of interfering a plane wave with a Laguerre–Gaussian beam would give rise to spiral fringes [36] rather than localized spots as in this case. Furthermore, in a 3D stationary Bessel lattice the axial confinement is achieved all-optically instead of magneto-optically. In addition, this lattice could also be a suitable choice for studies of atomic wavefunction interference between components that rotate in opposite directions.

Case 4: toroidal train lattice

The optical potential energy in this case corresponds to a set of toroidal cages aligned along the z-axis; the intensity pattern of the light field is shown in figure 4. In general, an atom initially

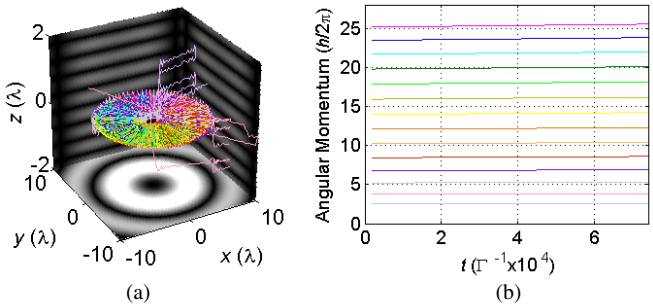

(a) (b)

Figure 8. (a) Spatial path of atoms moving within a toroidal Bessel lattice generated by the superposition of rotating BBs of second order propagating in opposite directions, as described in figure 4. (b) Angular momentum as a function of time for the same atoms. The parameters of the two superimposing beams and the range of initial conditions of the atoms in the analysed cloud are the same as those of figure 5. The colours of the illustrative paths in (a) are directly correlated to the angular momentum in (b).

located at an antinodal z plane ($z = n\lambda_z/2$) will remain trapped in a single torus, waving along the radial and axial directions and rotating around the beam axis, provided its total initial energy is negative. On the other hand, atoms initially located at a nodal surface may hop to neighbour toroidal traps either one way or the other, while keeping trapped in the radial direction and rotating around the beam axis. This hopping behaviour may be exhibited during relatively long time intervals ($t \approx 10^5\ \Gamma^{-1}$) before the atom finally escapes. Typical examples of paths followed by atoms of a cloud trapped in this lattice can be seen in figure 8(a). If an atom has a non-null azimuthal component of its initial velocity, it will remain rotating around the beam axis at practically constant average angular velocity. This can be appreciated from figure 8(b), where the angular momenta of the different atoms remain almost constant and have the same order of magnitude than in case 1 of the propagating rotating BB, which is much smaller than in the other two cases studied here.

5. 3D atom circuits with combination of Bessel lattices

With a clear picture of the mechanical behaviour of atoms in the different light fields we have discussed so far, we are in a position to elucidate a more sophisticated application. By alternating the operation of different lattices in an appropriated combination, it is possible to create what we call 'atom loops'. These loops can either be 'open' or 'closed'. By a 'closed' loop we do not mean, of course, that the atom will come back to its initial position, but rather to approximately the same spatial region.

For instance, consider a cloud of atoms downloaded into a toroidal train lattice. After a transitory time, we obtain a steady cloud of atoms trapped in the radial and axial directions moving essentially with their initial angular momentum. By applying the twisted helical Bessel lattice, they will move downwards or upwards depending on the helicity of the light field and the direction of the atomic azimuthal velocity. In general, the twisted helical lattice preserves the radial trapping and modifies the atomic angular momentum L_z. Now, by turning on a toroidal train lattice just after the twisted helical lattice is turned off, the atoms will be again axially trapped. If most of the atoms in the first toroidal lattice moved nearby the $z = 0$ plane, in the final configuration, we expect that most atoms rotating in toroidal cages with $z > 0$ will have an opposite angular momentum L_z to those rotating in cages with $z < 0$. We confirmed these ideas by performing several numerical simulations of the process. For instance, consider an atomic cloud with an initial average kinetic energy $\langle K_{\text{in}} \rangle \approx 10\ \mu$K and an initial angular momentum average $\langle |L_z| \rangle \approx 50\hbar$. The twisted helical lattice is applied during a time interval $\Delta T = 5 \times 10^4\ \Gamma^{-1}$. In the final configuration, in each toroidal cage, ~85% of the trapped atoms had a common direction of rotation about the z-axis. This direction was opposite for $z > 0$ and for $z < 0$. During the process, 10% of the atoms were radially lost.

With the current technology of spatial light modulators, the switching among different options of optical lattices may be performed at reasonably high speeds, limited only by the response time of the specific light modulation device. An experimental study on the interactive generation and switching of the light patterns analysed here will be reported elsewhere. Here we assume valid a sudden approximation in which the atoms do not modify their state of motion during the switching.

We analysed other loops. As expected, in all cases, the higher the number of steps to obtain a predesigned path, the lower the number of atoms in a cloud that are able to follow it. This can become an advantage of the procedure when the purpose is to select atoms with predetermined mechanical parameters.

As a particular example, let us consider the following five-step circuit: step (1): an atom cloud is trapped in a toroidal cage for a given time interval; step (2): a twisted helical Bessel lattice is applied with the proper helicity to send the atoms upwards (downwards) if $\dot{\varphi} > 0$ ($\dot{\varphi} < 0$); step (3): they are trapped again in a toroidal cage; step (4): they are sent downwards (upwards) using a twisted helical lattice with opposite helicity than that in step (2); step (5): they are trapped again by a toroidal cage. This circuit admits the possibility of obtaining closed atomic loops. This is illustrated in figure 9 for an atomic cloud that had an initial average kinetic energy $\langle K_{\text{in}} \rangle \approx 10\ \mu$K and an initial angular momentum $\langle |L_z| \rangle \approx 50\hbar$. The application time intervals for each step were optimized to obtain a closed loop for a small, 5%, subset of atoms corresponding to those with the larger initial radial position ($R \sim 6\lambda$). In the procedure, we observed that most radial loses occur in the first three steps. After that about 10% of the trajectories corresponded to closed loops. All those atoms had the same direction of rotation. Figure 9 illustrates an example of this loop, but other combinations can be explored for different purposes. Note that atoms with preselected energies and momenta could be guided in different directions, so that circuits could be designed with the possibility of performing atom interference experiments.

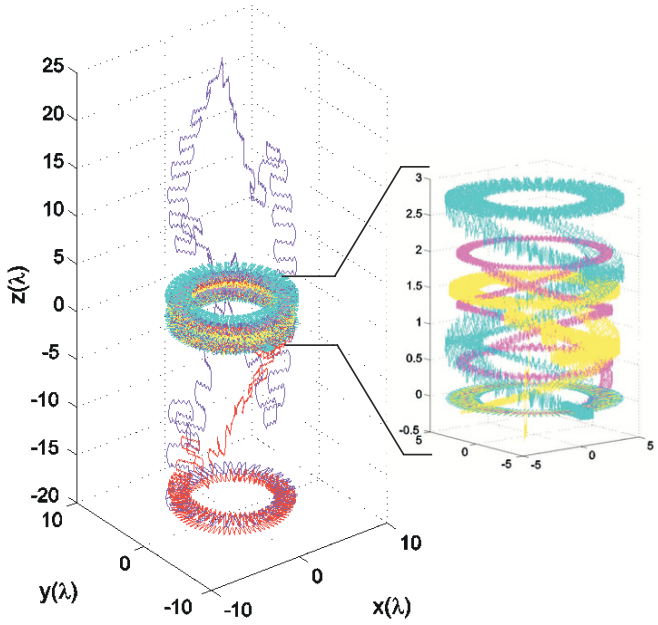

Figure 9. Some illustrative closed and open atom loops obtained by the effect of five different light fields operated consecutively: (1) toroidal, (2) twisted helical, (3) toroidal, (4) twisted helical with opposite helicity than in (2), (5) toroidal. The general parameters of the light fields correspond to those in figures (6) and (8). The initial average kinetic energy is $\langle K_{\text{in}}\rangle = 10\ \mu$K and the initial angular momentum is $\langle|L_z|\rangle 50\hbar$. The application times of each step were optimized to obtain a closed loop for atoms with initial conditions close to those of the blue trajectory. Most of the atoms performed 'open-loop' trajectories, such as the red or purple ones, since their final trajectory is not close to the initial one. However, radial looses were not too frequent during the whole procedure (about 15%) and most of them occur in the first three steps.

6. Conclusions

We have analysed the dynamical behaviour of an atomic cloud moving under the action of four different configurations of light fields with circular cylindrical geometry: a propagating–rotating Bessel beam of order m, a twisted helical lattice or twisted helical field, a 3D stationary circular lattice and a toroidal train lattice. We presented the fundamental equation for the optical force, based on [26, 34], and gave the specific expressions for the conservative $\vec{\alpha}$ and dissipative $\vec{\beta}$ terms of the force in each of the cases under study. In section 4, we discussed the numerical results, case by case, of the solution of the motion equations for the atom, for a red-detuned far-off-resonance system. We found that the single rotating Bessel beam and the twisted helical lattice can be used to guide atoms, in the latter case along $2|m|$ separate channels. In contrast, the 3D stationary circular lattice and the toroidal train lattice can be applied to obtain 3D confinement within a small region of the space. The twisted helical lattice can be used to select atomic helicities and gives rise to strong angular momentum oscillations. The 3D stationary circular lattice define a mean rotation axis for the atomic trajectories located at each potential cage. Finally, on the basis of our numerical results, we proposed an application consisting of the consecutive operation of the different options of light fields studied here, in order to create atom loops in predesigned ways by all-optical means.

Even when we have restricted our analysis here to the case of Bessel modes, it is worth appreciating that, in the paraxial versions, all the lattices or light fields discussed above would have an analogous in terms of Laguerre–Gaussian laser modes, which might be easier to generate experimentally. In that case, however, beam spreading on propagation should be taken into account; the waist plane of the interfering beams should coincide and the alignment may become an issue. Additionally, the beam spreading of Laguerre–Gaussian modes may prevent the formation of atomic loops in the sense defined above. In general, however, regardless of the specific form of the radial profile, any beam with circular cylindrical symmetry could be useful for generating similar lattices to those studied here, and the behaviour of cold atoms in such lattices is expected to be analogous to that discussed in this paper. It is worth mentioning as well that in the specific case of Bessel lattices with light irradiance of about 6 mW μm^{-2}, we found that atoms with initial kinetic energies of up to 30 μK can be trapped not only in the first ring of the Bessel profile, but also in the second and even in the third outer rings.

There are also very interesting features occurring in the cases of near-resonance conditions and blue-detuned systems that are by themselves worthy of other thorough studies. For instance, Gommers and coworkers considered near-resonance conventional lattices to experimentally generate an atomic ratchet [37]. The lattices studied here may represent very attractive novel options for this purpose, since one can generate quasiperiodic systems with open-boundary conditions along the z-axis, but also with closed-boundary conditions along the azimuthal coordinate, and ratchet systems with new geometries can be explored as well. Therefore, a possibility of performing novel studies on stochastic dynamics in atomic systems is opened both classically and quantum-mechanically, since atomic temperatures will define the proper dynamics. A quantum description of the dynamics of atoms in cylindrical beams will be reported elsewhere.

Acknowledgments

RJ thanks Professor J Recámier for useful discussions. This work was partially supported by DGAPA-UNAM, projects IN103103 and IN115307.

References

[1] Miller J D, Cline R A and Heinzen D J 1993 Far-off-resonance optical trapping of atoms *Phys. Rev.* A **47** R4567–70
[2] Jessen P S and Deutsch I H 1996 Optical lattices *Adv. Atm. Mol. Opt. Phys.* **37** 95–139
[3] Cornell E 1996 Very cold indeed: the nanokelvin physics of Bose–Einstein condensation *J. Res. Natl Inst. Stand. Technol.* **101** 419–36
[4] Inouye S, Pfau T, Gupta S, Chikkatur A P, Gorlitz A, Pritchard D E and Ketterle W 1999 Phase-coherent amplification of atomic matter waves *Nature* **402** 641–4
[5] Durnin J, Miceli J J and Eberly J H 1987 Diffraction-free beams *Phys. Rev. Lett.* **58** 1499–501

[6] Arlt J, Hitomi T and Dholakia K 2000 Atom guiding along Laguerre–Gaussian and Bessel light beams *Appl. Phys.* B **71** 549–54
[7] Arlt J, Dholakia K, Soneson J and Wright E M 2001 Optical dipole traps and atomic waveguides based on Bessel light beams *Phys. Rev.* A **63** 063602
[8] Rodríguez-Lara B M and Jáuregui R 2008 Dynamical constants for electromagnetic fields with elliptic-cylindrical symmetry *Phys. Rev.* A **78** 033813
[9] Allen L, Beijersbergen M W, Spreeuw R J C and Woerdman J P 1992 Orbital angular momentum of light and the transformation of Laguerre–Gaussian laser modes *Phys. Rev.* A **45** 8185–9
[10] Babiker M, Bennett C R, Andrews D L and Davila-Romero L C 2002 Orbital angular momentum exchange in the interaction of twisted light with molecules *Phys. Rev. Lett.* **89** 143601
[11] Volke-Sepúlveda K, Garcés-Chávez V, Chávez-Cerda S, Arlt J and Dholakia K 2002 Orbital angular momentum of a high-order Bessel light beam *J. Opt. B: Quantum Semiclass. Opt.* **4** S82–8
[12] Alexandrescu A, Cojoc D and Di Fabrizio E 2006 Mechanism of angular momentum exchange between molecules and Laguerre–Gaussian beams *Phys. Rev. Lett.* **96** 243001
[13] Jáuregui R 2004 Rotational effects of twisted light on atoms beyond the paraxial approximation *Phys. Rev.* A **70** 033415
[14] Jáuregui R and Hacyan S 2005 Quantum-mechanical properties of Bessel beams *Phys. Rev.* A **71** 033411
[15] Haroutyunyan H L and Nienhuis G 2004 Diffraction by circular optical lattices *Phys. Rev.* A **70** 063408
[16] Bhattacharya M 2007 Lattice with a twist: helical waveguides for ultracold matter *Opt. Commun.* **279** 219–22
[17] Paraoanu G S 2003 Persistent currents in a circular array of Bose–Einstein condensates *Phys. Rev.* A **67** 023607
[18] Amico L, Osterloh A and Cataliotti F 2005 Quantum many particle systems in ring-shaped optical lattices *Phys. Rev. Lett.* **95** 063201
[19] Olson S E, Terraciano M L, Bashkansky M and Fatemi F K 2007 Cold-atom confinement in an all-optical dark ring trap *Phys. Rev.* A **76** 061404R
[20] Schwartz S, Cozzini M, Menotti C, Carusotto I, Bouyer P and Stringari S 2006 One-dimensional description of a Bose–Einstein condensate in a rotating closed-loop waveguide *New J. Phys.* **8** 162
[21] Peden B M, Bhat R, Kramer M and Holland M J 2007 Quasi-angular momentum of Bose and Fermi gases in rotating optical lattices *J. Phys. B: At. Mol. Opt. Phys.* **40** 3725–44
[22] Tabosa J W R and Petrov D V 1999 Optical pumping of orbital angular momentum of light in cold cesium atoms *Phys. Rev. Lett.* **83** 4967–70
[23] Andersen M F, Ryu C, Clade P, Natarajan V, Vaziri A, Helmerson K and Phillips W D 2006 Quantized rotation of atoms from photons with orbital angular momentum *Phys. Rev. Lett.* **97** 170406
[24] Pugatch R, Shuker M, Firstenberg O, Ron A and Davidson N 2007 Topological stability of stored optical vortices *Phys. Rev. Lett.* **98** 203601
[25] Moretti D, Felinto D and Tabosa J W R 2009 Collapses and revivals of stored orbital angular momentum of light in a cold atomic ensemble arXiv:0901.0939v1
[26] Gordon J P and Ashkin A 1980 Motion of atoms in a radiation trap *Phys. Rev.* A **21** 1606–17
[27] Barnett S M and Allen L 1994 Orbital angular momentum and non-paraxial light-beams *Opt. Commun.* **110** 670–8
[28] Volke-Sepúlveda K and Ley-Koo E 2006 General construction and connections of vector propagation invariant optical fields: TE and TM modes and polarization states *J. Opt. A: Pure Appl. Opt.* **8** 867–77
[29] Bekshaev A Ya, Soskin M S and Vasnetsov M V 2005 Angular momentum of a rotating light beam *Opt. Commun.* **249** 367–78
[30] Nienhuis G 2006 Polychromatic and rotating beams of light *J. Phys. B: At. Mol. Opt. Phys.* **39** S529–44
[31] Arlt J and Dholakia K 2000 Generation of high-order Bessel beams by use of an axicon *Opt. Commun.* **177** 297–301
[32] Vasara A, Turunen J and Friberg A 1989 Realization of general nondiffracting beams with computer-generated holograms *J. Opt. Soc. Am.* A **6** 1748
[33] Davis J A, Guertin J and Cottrell D M 1993 Diffraction-free beams generated with programmable spatial light modulators *Appl. Opt.* **32** 6368–70
[34] Balykin V I, Minogin V G and Letokhov V S 2000 Electromagnetic trapping of cold atoms *Rep. Prog. Phys.* **63** 1429–510
[35] http://www.fisica.unam.mx/research/movies/
[36] MacDonald M P, Volke-Sepúlveda K, Paterson l, Arlt J, Sibbett W and Dholakia K 2002 Revolving interference patterns for the rotation of optically trapped particles *Opt. Commun.* **201** 21–8
[37] Gommers R, Denisov S and Renzoni F 2006 Quasiperiodically Driven Ratchets for cold atoms *Phys. Rev. Lett.* **96** 240604